

World Journal of *Radiology*

World J Radiol 2023 May 28; 15(5): 136-156



MINIREVIEWS

- 136 Future of prostate imaging: Artificial intelligence in assessing prostatic magnetic resonance imaging
Chervenkov L, Sirakov N, Kostov G, Velikova T, Hadjidekov G

ORIGINAL ARTICLE**Retrospective Cohort Study**

- 146 Chronic thromboembolic pulmonary hypertension is associated with a loss of total lung volume on computed tomography
Tsuchiya N, Xu YY, Ito J, Yamashiro T, Ikemiyagi H, Mummy D, Schiebler ML, Yonemoto K, Murayama S, Nishie A

ABOUT COVER

Associate Editor of *World Journal of Radiology*, Mina S Makary, MD, Assistant Professor, Director, Department of Radiology, The Ohio State University Wexner Medical Center, Columbus, OH 43210, United States. mina.makary@osumc.edu

AIMS AND SCOPE

The primary aim of *World Journal of Radiology* (*WJR*, *World J Radiol*) is to provide scholars and readers from various fields of radiology with a platform to publish high-quality basic and clinical research articles and communicate their research findings online.

WJR mainly publishes articles reporting research results and findings obtained in the field of radiology and covering a wide range of topics including state of the art information on cardiopulmonary imaging, gastrointestinal imaging, genitourinary imaging, musculoskeletal imaging, neuroradiology/head and neck imaging, nuclear medicine and molecular imaging, pediatric imaging, vascular and interventional radiology, and women's imaging.

INDEXING/ABSTRACTING

The *WJR* is now abstracted and indexed in PubMed, PubMed Central, Emerging Sources Citation Index (Web of Science), Reference Citation Analysis, China National Knowledge Infrastructure, China Science and Technology Journal Database, and Superstar Journals Database. The 2022 edition of Journal Citation Reports® cites the 2021 Journal Citation Indicator (JCI) for *WJR* as 0.48.

RESPONSIBLE EDITORS FOR THIS ISSUE

Production Editor: *Si Zhao*; Production Department Director: *Xu Guo*; Editorial Office Director: *Jia-Ping Yan*.

NAME OF JOURNAL

World Journal of Radiology

ISSN

ISSN 1949-8470 (online)

LAUNCH DATE

January 31, 2009

FREQUENCY

Monthly

EDITORS-IN-CHIEF

Thomas J Vogl

EDITORIAL BOARD MEMBERS

<https://www.wjgnet.com/1949-8470/editorialboard.htm>

PUBLICATION DATE

May 28, 2023

COPYRIGHT

© 2023 Baishideng Publishing Group Inc

INSTRUCTIONS TO AUTHORS

<https://www.wjgnet.com/bpg/gerinfo/204>

GUIDELINES FOR ETHICS DOCUMENTS

<https://www.wjgnet.com/bpg/GerInfo/287>

GUIDELINES FOR NON-NATIVE SPEAKERS OF ENGLISH

<https://www.wjgnet.com/bpg/gerinfo/240>

PUBLICATION ETHICS

<https://www.wjgnet.com/bpg/GerInfo/288>

PUBLICATION MISCONDUCT

<https://www.wjgnet.com/bpg/gerinfo/208>

ARTICLE PROCESSING CHARGE

<https://www.wjgnet.com/bpg/gerinfo/242>

STEPS FOR SUBMITTING MANUSCRIPTS

<https://www.wjgnet.com/bpg/GerInfo/239>

ONLINE SUBMISSION

<https://www.f6publishing.com>

Future of prostate imaging: Artificial intelligence in assessing prostatic magnetic resonance imaging

Lyubomir Chervenkov, Nikolay Sirakov, Gancho Kostov, Tsvetelina Velikova, George Hadjidekov

Specialty type: Radiology, nuclear medicine and medical imaging

Provenance and peer review:

Invited article; Externally peer reviewed.

Peer-review model: Single blind

Peer-review report's scientific quality classification

Grade A (Excellent): 0
Grade B (Very good): B, B
Grade C (Good): C, C
Grade D (Fair): D
Grade E (Poor): 0

P-Reviewer: Konovalov AB, Russia; Lei Y, China; Mijwil MM, Iraq

Received: December 19, 2022

Peer-review started: December 19, 2022

First decision: February 20, 2023

Revised: March 21, 2023

Accepted: April 10, 2023

Article in press: April 10, 2023

Published online: May 28, 2023



Lyubomir Chervenkov, Department of Diagnostic Imaging, Medical University Plovdiv, Plovdiv 4000, Bulgaria

Lyubomir Chervenkov, Nikolay Sirakov, Research Complex for Translational Neuroscience, Medical University of Plovdiv, Bul. Vasil Aprilov 15A, Plovdiv 4002, Bulgaria

Nikolay Sirakov, Department of Diagnostic Imaging, Dental Allergology and Physiotherapy, Faculty of Dental Medicine, Medical University Plovdiv, Plovdiv 4000, Bulgaria

Gancho Kostov, Department of Special Surgery, Medical University Plovdiv, Plovdiv 4000, Bulgaria

Tsvetelina Velikova, Department of Clinical Immunology, University Hospital Lozenetz, Sofia 1407, Bulgaria

Tsvetelina Velikova, Department of Medical Faculty, Sofia University St. Kliment Ohridski, Sofia 1407, Bulgaria

George Hadjidekov, Department of Radiology, University Hospital Lozenetz, Sofia 1407, Bulgaria

George Hadjidekov, Department of Physics, Biophysics and Radiology, Medical Faculty, Sofia University St. Kliment Ohridski, Sofia 1407, Bulgaria

Corresponding author: George Hadjidekov, MD, PhD, Associate Professor, Department of Radiology, University Hospital Lozenetz, 1 Kozyak Street, Sofia 1407, Bulgaria. jordiman76@yahoo.com

Abstract

Prostate cancer (Pca; adenocarcinoma) is one of the most common cancers in adult males and one of the leading causes of death in both men and women. The diagnosis of Pca requires substantial experience, and even then the lesions can be difficult to detect. Moreover, although the diagnostic approach for this disease has improved significantly with the advent of multiparametric magnetic resonance, that technology has certain unresolved limitations. In recent years artificial intelligence (AI) has been introduced to the field of radiology, providing new software solutions for prostate diagnostics. Precise mapping of the prostate has become possible through AI and this has greatly improved the accuracy of biopsy. AI has also allowed for certain suspicious lesions to be attributed to a given group according to the Prostate Imaging-Reporting & Data System classification. Finally,

AI has facilitated the combination of data obtained from clinical, laboratory (prostate-specific antigen), imaging (magnetic resonance), and biopsy examinations, and in this way new regularities can be found which at the moment remain hidden. Further evolution of AI in this field is inevitable and it is almost certain to significantly expand the efficacy, accuracy and efficiency of diagnosis and treatment of Pca.

Key Words: Artificial intelligence; Deep learning; Machine learning; Multiparametric magnetic resonance imaging; Prostate cancer; Quantitative imaging

©The Author(s) 2023. Published by Baishideng Publishing Group Inc. All rights reserved.

Core Tip: The peer reviewed literature has provided sufficient support for the continued application and development of artificial intelligence (AI) in prostate cancer clinical care. In addition, the expanding introduction of various AI-based software products created by leading companies is providing practical benefits to radiologists for improved prostate cancer diagnosis. Certainly, the known complexity of the disease and its consequential difficult diagnosis supports the continued development of new approaches for earlier and more accurate detection, such as could be provided through AI technologies.

Citation: Chervenkov L, Sirakov N, Kostov G, Velikova T, Hadjidekov G. Future of prostate imaging: Artificial intelligence in assessing prostatic magnetic resonance imaging. *World J Radiol* 2023; 15(5): 136-145

URL: <https://www.wjgnet.com/1949-8470/full/v15/i5/136.htm>

DOI: <https://dx.doi.org/10.4329/wjr.v15.i5.136>

INTRODUCTION

Prostate cancer (Pca; an adenocarcinoma) is one of the leading causes of death from oncological diseases, and it ranks second among adult males. Despite the high frequency of the disease, screening still largely relies on digital rectal examination, with low sensitivity and low specificity, and prostate-specific antigen (PSA) testing, with high sensitivity but low specificity. If the tests support a positive suspicion, a transrectal ultrasound (TRUS) biopsy is performed[1]. A Pca diagnosis is classified as either clinically significant, with the adenocarcinoma lesion requiring surgical treatment to curb the risk of metastasis, or non-significant, with follow-up recommended[2-4].

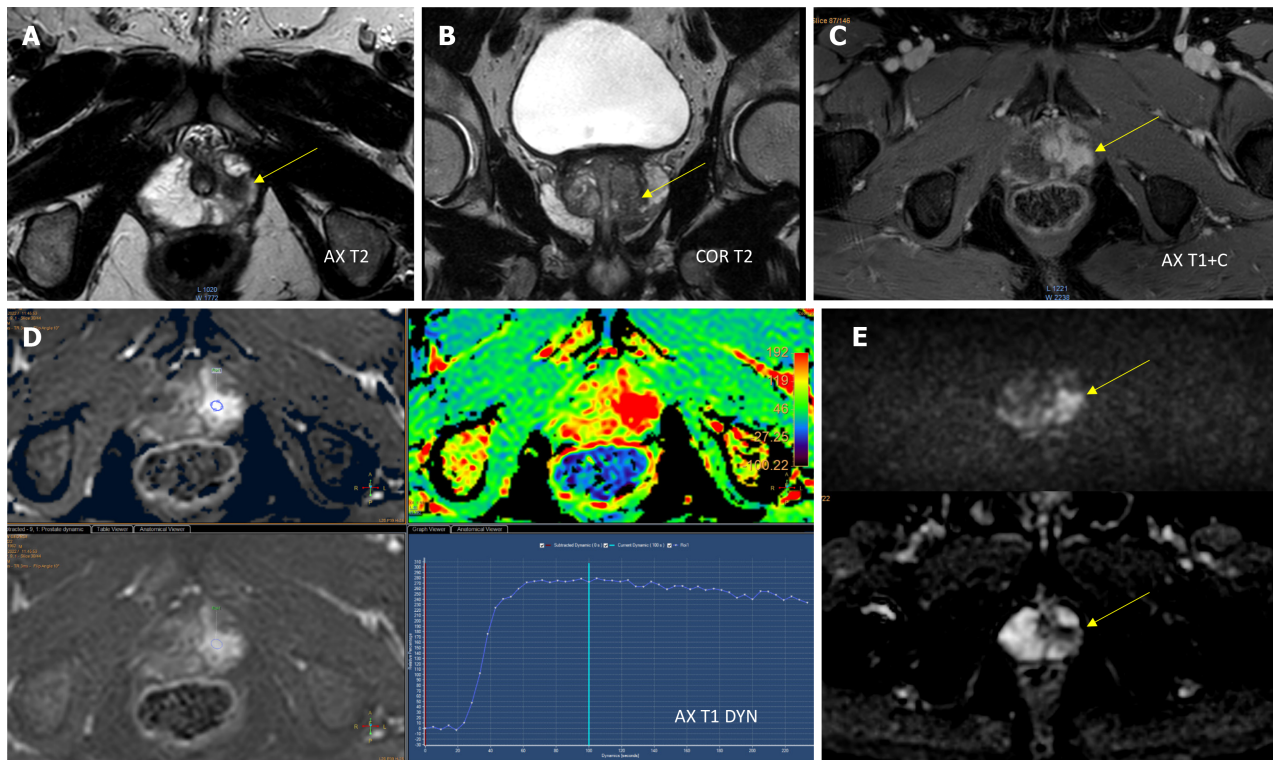
Multiparametric magnetic resonance imaging (mpMRI) is gaining ground as a primary method for Pca diagnosis. However, the diagnostic process requires a radiologist who has deep experiential knowledge with both the disease and the MRI technology[1-3,5]. The Prostate Imaging-Reporting & Data System (PI-RADS; introduced in 2012) and the 2.1 update (2019, with improved sensitivity and specificity) has begun to standardize the process by providing a classification system for findings detectable in Pca[6-8].

The mpMRI technology itself has opened up new opportunities for more accurate and earlier Pca detection (and diagnosis). It is specifically recommended for patients with elevated PSA levels but negative biopsy results and for biopsy-naïve patients who are being monitored for Pca due to risk factors (*e.g.*, age, family history, race). In addition, mpMRI is considered a safer alternative to the TRUS biopsy, as it avoids the complication risks related to the invasive biopsy procedure (*e.g.*, bleeding, infection, urinary hesitancy)[4].

Three-dimensional images of the prostate gland, including high-resolution T2-weighted image (WI), diffusion-weighted image (DWI) and dynamic contrast-enhanced (DCE) image, are obtained using mpMRI (Figure 1). The imaging findings are combined with the overall clinical profile to determine the level of risk for a clinically significant cancer, following the PI-RADS classification[4].

American and European guidelines differ from each other in their recommendations for the appropriate time of biopsy[9]. Gleason staging has proven to be an accurate approach, but it (as well as the PI-RADS) has significant limitations in diagnosis and quantification; for example, the PI-RADS system is known to risk provision of an underestimation of tumor size, especially in patients with a low PI-RADS score, while higher PI-RADS score is associated with Gleason score upgrade[10]. In addition, the inherent heterogeneity of Pca, known limitations of mpMRI, and possible biopsy inaccuracies can lead to inconsistencies in the overall assessment of the patient's condition.

Currently, the detection of a prostate carcinoma lesion depends to a large extent on the experience of the radiologist, and in some cases even experienced radiologists find it difficult to detect the lesion or to classify the detected lesion by PI-RADS. In addition, in many cases, hypertrophy of the prostate with age makes it impossible to accurately localize the lesion and consequently hinders the surgeon's ability to perform an accurate biopsy. It is also necessary to unify the description of a given lesion in relation to



DOI: 10.4329/wjr.v15.i5.136 Copyright ©The Author(s) 2023.

Figure 1 Apical peripheral zone with a Prostate Imaging-Reporting & Data System 5 lesion. A and B: Axial (A) and coronal (B) T2-weighted imaging (WI) revealed a homogeneous hypointense lesion in the anterior peripheral zone of the apex; C: Postcontrast axial T1WI showed pronounced enhancement of the lesion; D: Early dynamic contrast-enhanced imaging showed positive enhancement within the lesion and provided a wash-out signal intensity curve; E: Diffusion weighted imaging (DWI) and apparent diffusion coefficient (ADC) diffusion restriction [DWI ($b = 1000 \text{ s/mm}^2$)] provided a marked hyperintense signal above the background, while the ADC map image showed a lesion with hypointense signal below the background.

generally accepted templates. Fortunately, all these limitations can be overcome by the modern software technologies based on artificial intelligence (AI)[11].

CHALLENGES IN ASSESSING PROSTATIC MRI

The Pca detection process has its weaknesses at present. Indeed, prostate carcinoma lesions are often confused with prostatitis, benign nodules, or hemorrhagic nodules, especially in the transitional zone. This often results in unnecessary biopsies[12]. Another pitfall involves the histological assessment of the biopsied lesion, with inaccuracies resulting in dangerous false-negative findings or incorrect staging[13].

AI has been applied to various diseases in the fields of imaging diagnostics and pathological profiling, most often increasing the efficiency in evaluating results. Especially as with mpMRI, different AI-based solutions have been found to allow for accurate segmentation of the prostate as well as an accurate characterization of the tumors[14]. In the field of pathology, an improvement in diagnostics has also been observed. As with any disease that is managed clinically, a radiological-pathological correlation is required, and this presents an existing lacuna that AI can fill, and certainly biomarker data will play a role as well. Increased knowledge of the pathological mechanism, as can be supported by application of AI, is a crucial component to multidisciplinary clinical care (*i.e.* collaborative care teams of radiologists, pathologists, and urologists for Pca patients). Overall, this process of incorporating AI into any disease diagnosis will also aid in the discovery of hitherto hidden relationships between different pathology-related biomarkers[15,16].

AI IN MEDICINE

AI is a computer system that performs actions similar to human intelligence. In radiology, AI has developed rapidly in recent years due to the ability of the cutting-edge technology to automatically extract information. Machine learning a subfield of AI is an algorithm that is trained for specific tasks without human intervention, which means that computers can be trained from certain examinations that have been previously described by a radiologist according to their didactic knowledge and practical

experience. As more research data, including that involving AI, accumulates, the effectiveness of software increases. Human validation is still required, after which calibration is performed, resulting in better sensitivity and specificity of the novel/improved software. A subtype of machine learning is convolutional neural networks, where different systems interact with one another[17]. Of note, this type of system is the most frequently used in the development of AI[18].

AI has already shown great benefit in improving the detection, characterization, staging and participation in adequately treating Pca. Accurate prostate segmentation is particularly important when performing mpMRI, which without AI is relatively conditional on the perceptions of individual specialists. AI can be involved in the primary detection and staging of prostate carcinoma lesions relative to the PI-RADS system. A study by Cuocolo *et al*[14] published in 2021 investigated the characterization of human *vs* AI findings and demonstrated the benefit of the latter. In addition, AI can optimize the exact site for biopsy, as well as create a three-dimensional model to accurately represent the location of the tumor and its relationship to neighboring organs, improving preoperative preparation. Still other publications from recent years have shown regularity between the findings in T2, the changes in DWI, and the density of tissue composition, allowing for the creation of radiopathological maps[19-21].

AI has already proven its utility in other fields of medicine. For example, machine learning has been used in patients with appendicitis, emerging as a tool to predict whether the disease is acute or subacute; specifically, AI showed accurately predicted result in 83.75% of the cases, precision of 84.11%, sensitivity of 81.08%, and specificity of 81.01%[22]. In general, the ever-increasing role of precision medicine, the anticipated future improvements of machine learning and deep learning, and the ongoing expansion of robotics and radiomics are likely to facilitate the robust development of reproducible MRI-based prostatic diagnostics[23].

AI CHALLENGES

The greatest challenge to establishing AI in medical practice, at the moment, is the need for large volumes of data to be integrated into the AI systems. From a practical standpoint, this necessitates a large volume of time and effort from already-taxed radiologists with expertise in prostate imaging. Another challenge is that the collected data originate from different MRI devices made by various manufacturers with varying field strengths, and from studies performed using varying protocols. Ultimately, this means that studies should be grouped according to these varying features. Considering this issue, a study by Gaur *et al*[24] has shown the AI can not only reduce the time of interpretation of MRI findings from various machines but also improve the sensitivity (from 78% to 83.8% specifically), especially when radiologists with less experience in the field were using the technologies.

CURRENT AI PRODUCTS AVAILABLE

The diagnosis of Pca involves initial detection and accurate classification of the lesion(s) finding, and it is to these processes that software companies have directed their focus. AI systems are "trained" to detect cancer by inputting voluminous data from leading experts. Several groups are reporting various AI models for prostate segmentation, intraprostatic lesion detection and classification tasks with auspicious results[25].

Improvements are being sought in the detection of prostate carcinoma lesions that are invisible to human perception, thereby increasing early diagnosis[26-29]. In [Table 1](#), the current AI products in the prostate field are summarized[30].

"AI-Rad companion prostate MR" by Siemens Medical Solutions (Malvern, PA, United States) aids the fusion between MRI and ultrasound. Performing an ultrasound-guided biopsy alone carries risks such as hemorrhage, infection, and abscessation. Furthermore, the procedure may not provide an answer to the presence of carcinoma in a given patient if performed solely, without previous physical examination and application of other imaging modalities. At the same time, performing an mpMRI scan cannot provide a histological diagnosis. The modern model of Pca diagnosis includes an ultrasound examination in combination with a previously performed MR scan. The lesions found on the MR scan are described by a radiologist, after which the images are superimposed on the ultrasound machine and a fusion between the two methods is achieved. AI in this case assists the biopsy by applying automated segmentation of the prostate, thus saving time and increasing accuracy of the biopsy. The collaboration between the urologist and the radiologist is also improved, as it allows for additional targeting of the lesions detected by MR[31].

Another Siemens product is the "Prostate MR" tool (Siemens Healthineers, Cary, NC, United States), which is available on the syngo.via workstation and is an AI that supports the evaluation of images obtained during a mpMRI scan. Analysis time needed for the AI is extremely short - between 3 sec and 10 sec. Prostate MR supports the primary detection and classification of findings, and offers description according to pre-entered standardized report templates. The use of this type of software is extremely

Table 1 Current artificial intelligence products available in the prostate imaging field

Vendor	Product name	FDA approval class	CE approval class	Main features in prostate imaging
Siemens Healthineers	AI-Rad Companion Prostate MR	II	I Ib - MDR	Segmentation, volume assessment, lesion annotation, PSA density
Quantib	Quantib [®] Prostate	II	I Ib - MDR	Volume assessment, PSA density, segmentation, PI-RADS scoring, report structure
Quibim	QP-Prostate	II	I Ib - MDR	ADC, K ^{trans} , parametric maps obtainment, volume assessment, segmentation, report structure
Quibim	Perfusion pharmacokinetics modeling	N/A	I Ia - MDD	K ^{trans} map, volume assessment, contrast enhancement assistance
Quibim	Texture analysis	N/A	I Ia - MDD	Quantification, radiomics, imaging biomarker discovery
Quibim	T2 mapping (relaxometry)	N/A	I Ia - MDD	T2 values, T2 histogram
Siemens Healthineers	Prostate MR on syngo.via	N/A	I Ia - MDD	Segmentation, volume assessment, lesion assessment, PI-RADS scoring
JLK Inc.	JPC-01K	N/A	I - MDD	Lesion detection
Lucida Medical	Prostate Intelligence™	N/A	I - MDD	Segmentation, lesion characterization, PI-RADS scoring, report structure
Quibim	DWI - ADC	N/A	I Ia - MDD	Volume assessment, ADC support, histogram
Quibim	DWI - IVIM	N/A	I Ia - MDD	ADC support, multiparametric maps, perfusion assessment

ADC: Apparent diffusion coefficient; AI: Artificial intelligence; CE: Single Market in the European economic area; DWI: Diffusion weighted imaging; FDA: Food and Drug Administration; IVIM: Intravoxel incoherent motion; JPC-01K: An artificial intelligence-based prostate cancer detection solution; K^{trans}: Volume transfer constant; MDD: Medical Devices Directive; MDR: Medical device regulation; MR: Magnetic resonance; N/A: Not applicable; PI-RADS: Prostate Imaging-Reporting & Data System; PSA: Prostate-specific antigen.

valuable for training radiologists without experience in prostate diagnostics. Indeed, it has been reported that the software application leads to a reduction of false-positive results[32].

With the advent of mpMRI, the total number of examinations performed has increased significantly worldwide[33]. Radiologists today have to interpret multiple MRI scans of the prostate, but this requires great expertise in this challenging field. New guidelines from the European Association of Urology and the American Association of Radiology suggest that an MRI be performed before any biopsy is undertaken, and currently the number of prostate biopsies in the United States and Europe alone is over 3 million[33]. Eventual involvement of AI in the interpretation algorithm may improve the detection rate, accurate localization and risk stratification of patients with suspected Pca. "Quantib[®] Prostate" software (Quantib, Rotterdam, Netherlands) offers fast and automated segmentation of the prostate and detection of findings on the most used mpMRI sequences [T2WI, apparent diffusion coefficient (ADC), DWI, DCE]. The software also provides assistance in the PI-RADS classification of a discovery. Finally, with the help of the software, a standardized report can be written based on pre-created templates, thereby saving time and improving the quality of the report.

DCE perfusion imaging identifies tumors according to their vessel characteristics. The Pharmacokinetic Model used in Quantib[®] Prostate helps detect neoplasms and quantifies tumor neoangiogenesis to stage cancer aggressiveness. This suite supports the characterization of tumoral processes in the early detection, diagnosis, treatment response evaluation and follow-up of patients with cancer. The software assesses the characteristics of the tissues, provides T2WI mapping, and depicts the changes according to segmentation. The information obtained allows for the assessment and monitoring of solid tumors, such as prostate, rectal, and liver lesions[31].

"JPC-01K" (JLK Inc., Seoul, Korea) is a neural network-based software used to characterize tumors on mpMRI. This software aims to reduce the time needed to evaluate the prostate examination findings and assist in the description of such by providing quantitative analysis. It also aims to overcome the difficulties in image analysis, which are largely dependent on the radiologist and his/her qualifications and experience. The system uses mpMR images, T2WI, DWI, and DCE as input and visualizes the location of prostate carcinoma lesions and related probabilities. According to a study carried out in one center, the accuracy of the method was 99.65%, with a time required for analysis of only 2 min. The AI at this manufacturer undergoes constant improvement through the addition of new data from leading experts.

“Prostate Intelligence™” (Lucida Medical, Cambridge, United Kingdom) is AI-based software that allows prostate tumor detection on MR images. It is intended to augment a radiologist's interpretation of prostate MRI by providing a risk score and prostate segmentation, and aiding in lesion identification and segmentation. The processing time for this software is between 1 sec and 10 sec. The DWI algorithm by Quibim (Valencia, Spain) calculates the ADC. The suite provides information on the cellular and microstructural organization of tissues and highlights the relationship between pathological changes and the diffusion of water molecules. In addition, this suite aims to characterize tumoral processes to support early detection, diagnosis, treatment response evaluation and follow-up of patients.

The DWI algorithm by Quibim is also used to analyze the microstructure changes according to intra-voxel incoherent motion. The tool allows for the differentiation of pure diffusion changes due to variations in the vascular component and offers additional information complementary to conventional ADC results. This suite aims to characterize tumoral processes to support early detection, diagnosis, treatment response evaluation and follow-up of patients[31].

For timely detection, accurate diagnosis and proper treatment of the patient, we offer the algorithm presented in [Figure 2](#).

OPPORTUNITIES

Creating teams of radiologists and pathologists to jointly decide on the most accurate diagnosis and most effective and efficient treatment methods of patients with Pca would create a more efficient approach to clinical management of the disease to achieve the most successful outcome. With the help of AI, specialists from both fields can join forces, especially when making decisions about suspicious lesions classified as PI-RADS 3. It is possible to bring together in one system all critical components disease history, PSA levels, findings from imaging studies, genetic tests, laboratory tests, physical and histological exams, and treatment(s) performed. AI can facilitate the ability to analyze all these components and compare them to databases for risk stratification and better predictability[34,35].

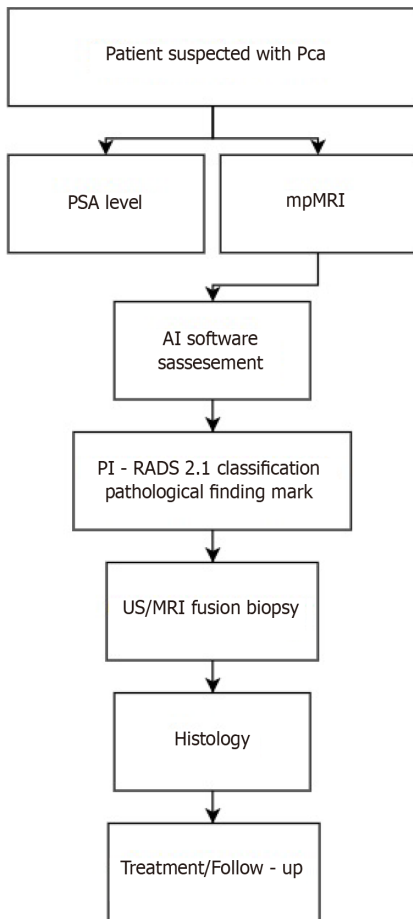
Positron emission tomography/computed tomography

Unlike most other carcinomas, the application of 18F-fluorodeoxyglucose (FDG) in positron emission tomography/computed tomography (PET/CT) is limited for Pca, due to the low or missing glucose consumption that is typically presented by prostate carcinoma lesions. Thus, the use of specific targeting is required. Until recently, choline was considered a promising marker (since choline uptake/concentration is high in prostatic carcinoma lesion cells). While this radioactive indicator was originally used for staging of high-risk patients as well as re-staging after biochemical relapse, its low sensitivity led to its largely being abandoned. Other markers such as 11C-acetate, 18F-oorocyclobutan-1-carboxylic acid and 18F-ucicloviore have been tested but have failed to meet expectations, presenting the same characteristics as choline and low sensitivity.

The prostate-specific membrane antigen (PSMA) currently dominates all other markers in PET scans for Pca. PSMA, also known as glutamate carboxypeptidase II, is a transmembrane glycoprotein, highly expressed in prostatic carcinoma lesion cells. PSMA expression tends to increase as Gleason score increases. So far, several ⁶⁸Ga (⁶⁸GA)-labeled ligands have been designed to target PSMA; these include PSMA-11 (known as Hbed-Cc or Hbed-PSMA), PSMA-I & T, and PSMA-617. Therefore, a ⁶⁸germanium (GE)/⁶⁸GA generator with T1/2WI of 271 d is widely used ([Figure 3](#)). However, with cyclotron access, PSMA-1007 looks like a substantial breakthrough as it shows an advantage over ⁶⁸GA-labeled PSMA markers.

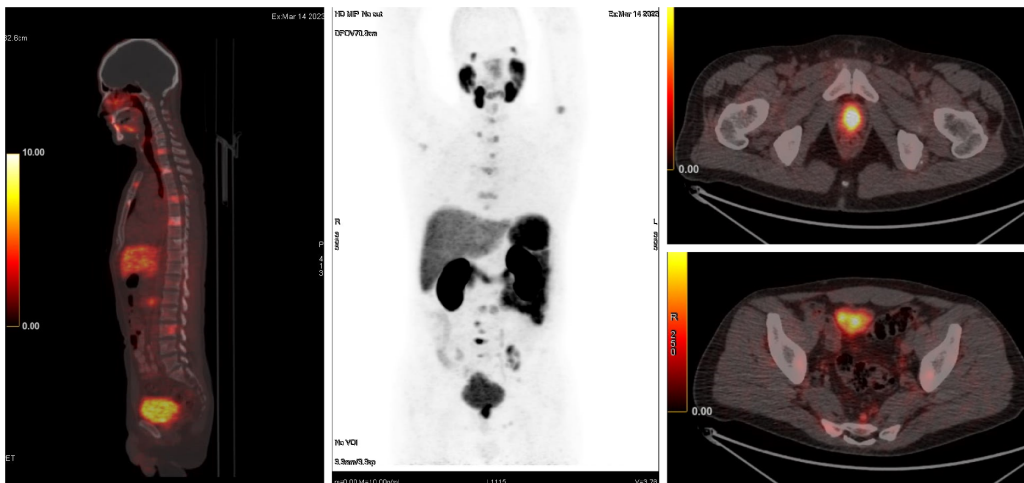
Multiple studies have shown that PET/CT with PSMA has a moderate sensitivity but a very high specificity for detecting metastases in lymph nodes and other organs. If the primary Pca shows PSMA expression, then a PSMA+ and PSMA- finding will be characterized as a secondary lesion or will be treated accordingly as a minor/benign lesion in the fragment imaging, although with the caveat of having high negative prognostic value. Due to the high monetary cost of PSMA studies, careful selection of patients suitable for examination is required. The mpMRI is superior for local assessment of the disease, and PSMA PET/MRI has an advantage in whole-body scanning. However, several restrictions are noted for patients suffering from Pca. For one, PET cameras are not always available and are missing in some of the nuclear medicine departments, especially in remote regions, for various logistical reasons. Another limitation is based in the fact that PSMA is not currently included in international guidelines. Lastly, although the utility of PSMA PET/CT in diagnosis of Pca is indisputable (outperforming diagnostics based solely on PSA, CT, and TRUS biopsy[36-40]) its role in monitoring of the disease remains unresolved.

Currently, only the “Pylarify AI™” software (Lantheus, Billerica, MA, United States) is legalized for support in PSMA PET/CT examinations, according to its demonstrated quantitative and accurate reporting. The AI software allows automated analysis of the CT examination's findings and allowing for targeting of the hotspots[41,42].



DOI: 10.4329/wjr.v15.i5.136 Copyright ©The Author(s) 2023.

Figure 2 Prostate cancer diagnosis algorithm. AI: Artificial intelligence; mpMRI: Multiparametric magnetic resonance imaging; MRI: Magnetic resonance imaging; Pca: Prostate cancer; PI-RADS: Prostate Imaging-Reporting & Data System; PSA: Prostate-specific antigen; US: Ultrasound.



DOI: 10.4329/wjr.v15.i5.136 Copyright ©The Author(s) 2023.

Figure 3 ⁶⁸Ga prostate-specific membrane antigen positron emission tomography-computed tomographic images for a patient with prostate cancer (adenocarcinoma). The imaging revealed a primary tumor and diffuse lymph node metastatic spread as well as multiple spinal metastases.

CONCLUSION

The increased incidence of Pca in recent years and the improvement of MRI technologies have led to an increase in the number of the examinations performed on patients for diagnosis of the disease. The larger volume of data that has resulted, combined with the insufficient number and/or insufficiently trained personnel, has unfortunately complicated the clinical process and management of these patients.

AI is a powerful modern tool that offers benefits of time reduction and improved quality and accuracy of interpretation of prostatic carcinoma lesion findings according to the unified PI-RADS system. AI application to the field of radiological imaging may revolutionize the approach to Pca patients. However, there is still a long way to go until we are able to fully calibrate the individual components of the new AI-based software solutions and carry out accurate and thorough studies in this arena to gain a comprehensive understanding of the pathology of the disease and clinical care benefits of this powerful tool.

ACKNOWLEDGEMENTS

The authors are grateful for the support provided by NextGenerationEU.

FOOTNOTES

Author contributions: Chervenkov L, Velikova T and Hadjidekov G conceptualized the study; Chervenkov L, Sirakov N and Kostov G designed the methodology; Chervenkov L performed the data curation; Chervenkov L prepared the original draft of the manuscript; Velikova T and Hadjidekov G reviewed and edited the manuscript for intellectual content; All authors contributed to manuscript revision and provided approval of the final version of the manuscript to be published.

Supported by the European Union's NextGenerationEU, through the National Recovery and Resilience Plan of the Republic of Bulgaria, Project No. BG-RRP-2.004-0008-C01.

Conflict-of-interest statement: All the authors report having no relevant conflicts of interest for this article.

Open-Access: This article is an open-access article that was selected by an in-house editor and fully peer-reviewed by external reviewers. It is distributed in accordance with the Creative Commons Attribution NonCommercial (CC BY-NC 4.0) license, which permits others to distribute, remix, adapt, build upon this work non-commercially, and license their derivative works on different terms, provided the original work is properly cited and the use is non-commercial. See: <https://creativecommons.org/licenses/by-nc/4.0/>

Country/Territory of origin: Bulgaria

ORCID number: Lyubomir Chervenkov 0000-0002-8380-5992; Nikolay Sirakov 0000-0002-2791-959X; Gancho Kostov 0000-0001-5137-6903; Tsvetelina Velikova 0000-0002-0593-1272; George Hadjidekov 0000-0001-6917-9887.

Corresponding Author's Membership in Professional Societies: European Society of Radiology (ESR); Bulgarian Association of Radiology (BAR); European Society of Uroradiology (ESUR); European Society of Gastroabdominal Radiology (ESGAR).

S-Editor: Liu XF

L-Editor: Filipodia

P-Editor: Zhao S

REFERENCES

- 1 **Ferlay J**, Colombet M, Soerjomataram I, Mathers C, Parkin DM, Piñeros M, Znaor A, Bray F. Estimating the global cancer incidence and mortality in 2018: GLOBOCAN sources and methods. *Int J Cancer* 2019; **144**: 1941-1953 [PMID: 30350310 DOI: 10.1002/ijc.31937]
- 2 **Fenton JJ**, Weyrich MS, Durbin S, Liu Y, Bang H, Melnikow J. Prostate-Specific Antigen-Based Screening for Prostate Cancer: Evidence Report and Systematic Review for the US Preventive Services Task Force. *JAMA* 2018; **319**: 1914-1931 [PMID: 29801018 DOI: 10.1001/jama.2018.3712]
- 3 **Hayes JH**, Barry MJ. Screening for prostate cancer with the prostate-specific antigen test: a review of current evidence. *JAMA* 2014; **311**: 1143-1149 [PMID: 24643604 DOI: 10.1001/jama.2014.2085]
- 4 **Doykov M**, Chervenkov, L., Tsvetkova-Trichkova, S., Doykova, K., Georgiev, A. Assessment of the Utility of Multiparametric Magnetic Resonance Imaging for Initial Detection of Prostate Cancer. *Macedonian Journal of Medical Sciences* 2022; **10**: 1840-1845 [DOI: 10.3889/oamjms.2022.10401]
- 5 **Barbieri CE**, Bangma CH, Bjartell A, Catto JW, Culig Z, Grönberg H, Luo J, Visakorpi T, Rubin MA. The mutational landscape of prostate cancer. *Eur Urol* 2013; **64**: 567-576 [PMID: 23759327 DOI: 10.1016/j.eururo.2013.05.029]
- 6 **Rosenkrantz AB**, Ayoola A, Hoffman D, Khasgiwala A, Prabhu V, Smereka P, Somberg M, Taneja SS. The Learning Curve in Prostate MRI Interpretation: Self-Directed Learning Versus Continual Reader Feedback. *AJR Am J Roentgenol* 2017; **208**: W92-W100 [PMID: 28026201 DOI: 10.2214/AJR.16.16876]
- 7 **Turkbey B**, Rosenkrantz AB, Haider MA, Padhani AR, Villeirs G, Macura KJ, Tempany CM, Choyke PL, Cornud F,

- Margolis DJ, Thoeny HC, Verma S, Barentsz J, Weinreb JC. Prostate Imaging Reporting and Data System Version 2.1: 2019 Update of Prostate Imaging Reporting and Data System Version 2. *Eur Urol* 2019; **76**: 340-351 [PMID: 30898406 DOI: 10.1016/j.eururo.2019.02.033]
- 8 **Georgiev A**, Chervenkov L, Doykov M, Doykova K, Uchikov P, Tsvetkova S. Surveillance Value of Apparent Diffusion Coefficient Maps: Multiparametric MRI in Active Surveillance of Prostate Cancer. *Cancers (Basel)* 2023; **15** [PMID: 36831471 DOI: 10.3390/cancers15041128]
 - 9 **Schoots IG**, Padhani AR. Delivering Clinical impacts of the MRI diagnostic pathway in prostate cancer diagnosis. *Abdom Radiol (NY)* 2020; **45**: 4012-4022 [PMID: 32356003 DOI: 10.1007/s00261-020-02547-x]
 - 10 **Pooli A**, Johnson DC, Shirk J, Markovic D, Sadun TY, Sisk AE Jr, Mohammadian Bajgiran A, Afshari Mirak S, Felker ER, Hughes AK, Raman SS, Reiter RE. Predicting Pathological Tumor Size in Prostate Cancer Based on Multiparametric Prostate Magnetic Resonance Imaging and Preoperative Findings. *J Urol* 2021; **205**: 444-451 [PMID: 33026934 DOI: 10.1097/JU.0000000000001389]
 - 11 **Aggarwal K**. Machine Learning, and Deep Learning. *Iraqi Journal for Computer Science and Mathematics* 2022; **3**: 115-123 [DOI: 10.52866/ijcsm.2022.01.01.013]
 - 12 **Loeb S**, Vellekoop A, Ahmed HU, Catto J, Emberton M, Nam R, Rosario DJ, Scattoni V, Lotan Y. Systematic review of complications of prostate biopsy. *Eur Urol* 2013; **64**: 876-892 [PMID: 23787356 DOI: 10.1016/j.eururo.2013.05.049]
 - 13 **Etzioni R**, Penson DF, Legler JM, di Tommaso D, Boer R, Gann PH, Feuer EJ. Overdiagnosis due to prostate-specific antigen screening: lessons from U.S. prostate cancer incidence trends. *J Natl Cancer Inst* 2002; **94**: 981-990 [PMID: 12096083 DOI: 10.1093/jnci/94.13.981]
 - 14 **Cuocolo R**, Cipullo MB, Stanzone A, Romeo V, Green R, Cantoni V, Ponsiglione A, Ugga L, Imbriaco M. Machine learning for the identification of clinically significant prostate cancer on MRI: a meta-analysis. *Eur Radiol* 2020; **30**: 6877-6887 [PMID: 32607629 DOI: 10.1007/s00330-020-07027-w]
 - 15 **Goldenberg SL**, Nir G, Salcudean SE. A new era: artificial intelligence and machine learning in prostate cancer. *Nat Rev Urol* 2019; **16**: 391-403 [PMID: 31092914 DOI: 10.1038/s41585-019-0193-3]
 - 16 **Raciti P**, Sue J, Ceballos R, Godrich R, Kunz JD, Kapur S, Reuter V, Grady L, Kanan C, Klimstra DS, Fuchs TJ. Novel artificial intelligence system increases the detection of prostate cancer in whole slide images of core needle biopsies. *Mod Pathol* 2020; **33**: 2058-2066 [PMID: 32393768 DOI: 10.1038/s41379-020-0551-y]
 - 17 **Park SH**, Han K. Methodologic Guide for Evaluating Clinical Performance and Effect of Artificial Intelligence Technology for Medical Diagnosis and Prediction. *Radiology* 2018; **286**: 800-809 [PMID: 29309734 DOI: 10.1148/radiol.2017171920]
 - 18 **Yilmaz EC**, Belue MJ, Turkbey B, Reinhold C, Choyke PL. A Brief Review of Artificial Intelligence in Genitourinary Oncological Imaging. *Can Assoc Radiol J* 2022; 8465371221135782 [PMID: 36515576 DOI: 10.1177/08465371221135782]
 - 19 **McGarry SD**, Hurrell SL, Iczkowski KA, Hall W, Kaczmarowski AL, Banerjee A, Keuter T, Jacobsohn K, Bukowy JD, Nevalainen MT, Hohenwarter MD, See WA, LaViolette PS. Radio-pathomic Maps of Epithelium and Lumen Density Predict the Location of High-Grade Prostate Cancer. *Int J Radiat Oncol Biol Phys* 2018; **101**: 1179-1187 [PMID: 29908785 DOI: 10.1016/j.ijrobp.2018.04.044]
 - 20 **Chatterjee A**, Bourne RM, Wang S, Devaraj A, Gallan AJ, Antic T, Karczmar GS, Oto A. Diagnosis of Prostate Cancer with Noninvasive Estimation of Prostate Tissue Composition by Using Hybrid Multidimensional MR Imaging: A Feasibility Study. *Radiology* 2018; **287**: 864-873 [PMID: 29393821 DOI: 10.1148/radiol.2018171130]
 - 21 **Chatterjee A**, Watson G, Myint E, Sved P, McEntee M, Bourne R. Changes in Epithelium, Stroma, and Lumen Space Correlate More Strongly with Gleason Pattern and Are Stronger Predictors of Prostate ADC Changes than Cellularity Metrics. *Radiology* 2015; **277**: 751-762 [PMID: 26110669 DOI: 10.1148/radiol.2015142414]
 - 22 **Mijwil MM**, Aggarwal K. A diagnostic testing for people with appendicitis using machine learning techniques. *Multimed Tools Appl* 2022; **81**: 7011-7023 [PMID: 35095329 DOI: 10.1007/s11042-022-11939-8]
 - 23 **Hamm CA**, Beetz NL, Savic LJ, Penzkofer T. [Artificial intelligence and radiomics in MRI-based prostate diagnostics]. *Radiologe* 2020; **60**: 48-55 [PMID: 31802148 DOI: 10.1007/s00117-019-00613-0]
 - 24 **Gaur S**, Lay N, Harmon SA, Doddakashi S, Mehrlivand S, Argun B, Barrett T, Bednarova S, Girometti R, Karaarslan E, Kural AR, Oto A, Puryrsko AS, Antic T, Magi-Galluzzi C, Saglican Y, Sioletic S, Warren AY, Bittencourt L, Fütterer JJ, Gupta RT, Kabakus I, Law YM, Margolis DJ, Shebel H, Westphalen AC, Wood BJ, Pinto PA, Shih JH, Choyke PL, Summers RM, Turkbey B. Can computer-aided diagnosis assist in the identification of prostate cancer on prostate MRI? a multi-center, multi-reader investigation. *Oncotarget* 2018; **9**: 33804-33817 [PMID: 30333911 DOI: 10.18632/oncotarget.26100]
 - 25 **Belue MJ**, Turkbey B. Tasks for artificial intelligence in prostate MRI. *Eur Radiol Exp* 2022; **6**: 33 [PMID: 35908102 DOI: 10.1186/s41747-022-00287-9]
 - 26 **Winkel DJ**, Wetterauer C, Matthias MO, Lou B, Shi B, Kamen A, Comaniciu D, Seifert HH, Rentsch CA, Boll DT. Autonomous Detection and Classification of PI-RADS Lesions in an MRI Screening Population Incorporating Multicenter-Labeled Deep Learning and Biparametric Imaging: Proof of Concept. *Diagnostics (Basel)* 2020; **10** [PMID: 33202680 DOI: 10.3390/diagnostics10110951]
 - 27 **Aldoj N**, Lukas S, Dewey M, Penzkofer T. Semi-automatic classification of prostate cancer on multi-parametric MR imaging using a multi-channel 3D convolutional neural network. *Eur Radiol* 2020; **30**: 1243-1253 [PMID: 31468158 DOI: 10.1007/s00330-019-06417-z]
 - 28 **Mehralivand S**, Yang D, Harmon SA, Xu D, Xu Z, Roth H, Masoudi S, Sanford TH, Kesani D, Lay NS, Merino MJ, Wood BJ, Pinto PA, Choyke PL, Turkbey B. A Cascaded Deep Learning-Based Artificial Intelligence Algorithm for Automated Lesion Detection and Classification on Biparametric Prostate Magnetic Resonance Imaging. *Acad Radiol* 2022; **29**: 1159-1168 [PMID: 34598869 DOI: 10.1016/j.acra.2021.08.019]
 - 29 **Winkel DJ**, Tong A, Lou B, Kamen A, Comaniciu D, Disselhorst JA, Rodríguez-Ruiz A, Huisman H, Szolar D, Shabunin I, Choi MH, Xing P, Penzkofer T, Grimm R, von Busch H, Boll DT. A Novel Deep Learning Based Computer-Aided Diagnosis System Improves the Accuracy and Efficiency of Radiologists in Reading Biparametric Magnetic Resonance

- Images of the Prostate: Results of a Multireader, Multicase Study. *Invest Radiol* 2021; **56**: 605-613 [PMID: 33787537 DOI: 10.1097/RLI.0000000000000780]
- 30 **Greer MD**, Shih JH, Lay N, Barrett T, Bittencourt L, Borofsky S, Kabakus I, Law YM, Marko J, Shebel H, Merino MJ, Wood BJ, Pinto PA, Summers RM, Choyke PL, Turkbey B. Interreader Variability of Prostate Imaging Reporting and Data System Version 2 in Detecting and Assessing Prostate Cancer Lesions at Prostate MRI. *AJR Am J Roentgenol* 2019; **212**: 1197-1205 [PMID: 30917023 DOI: 10.2214/AJR.18.20536]
- 31 **Strohm L**, Hehakaya C, Ranschaert ER, Boon WPC, Moors EHM. Implementation of artificial intelligence (AI) applications in radiology: hindering and facilitating factors. *Eur Radiol* 2020; **30**: 5525-5532 [PMID: 32458173 DOI: 10.1007/s00330-020-06946-y]
- 32 **Yu X**. False Positive Reduction Using Multiscale Contextual Features for Prostate Cancer Detection in Multi-Parametric MRI Scans. *IEEE 17th International Symposium on Biomedical Imaging (ISBI) 2020*; 1355-1359 [DOI: 10.1109/ISBI45749.2020.9098338]
- 33 **Mottet N**, van den Bergh RCN, Briers E, Van den Broeck T, Cumberbatch MG, De Santis M, Fanti S, Fossati N, Gandaglia G, Gillessen S, Grivas N, Grummet J, Henry AM, van der Kwast TH, Lam TB, Lardas M, Liew M, Mason MD, Moris L, Oprea-Lager DE, van der Poel HG, Rouvière O, Schoots IG, Tilki D, Wiegel T, Willemsse PM, Cornford P. EAU-EANM-ESTRO-ESUR-SIOG Guidelines on Prostate Cancer-2020 Update. Part 1: Screening, Diagnosis, and Local Treatment with Curative Intent. *Eur Urol* 2021; **79**: 243-262 [PMID: 33172724 DOI: 10.1016/j.eururo.2020.09.042]
- 34 **van Wijk Y**, Halilaj I, van Limbergen E, Walsh S, Lutgens L, Lambin P, Vanneste BGL. Decision Support Systems in Prostate Cancer Treatment: An Overview. *Biomed Res Int* 2019; **2019**: 4961768 [PMID: 31281840 DOI: 10.1155/2019/4961768]
- 35 **Lee G**, Singanamalli A, Wang H, Feldman MD, Master SR, Shih NN, Spangler E, Rebbeck T, Tomaszewski JE, Madabhushi A. Supervised multi-view canonical correlation analysis (sMVCCA): integrating histologic and proteomic features for predicting recurrent prostate cancer. *IEEE Trans Med Imaging* 2015; **34**: 284-297 [PMID: 25203987 DOI: 10.1109/TMI.2014.2355175]
- 36 **Hahn P**, Smith IC, Leboldus L, Littman C, Somorjai RL, Bezabeh T. The classification of benign and malignant human prostate tissue by multivariate analysis of 1H magnetic resonance spectra. *Cancer Res* 1997; **57**: 3398-3401 [PMID: 9270004]
- 37 **Tsichelidis I**, Vrachimis A. PSMA PET in Imaging Prostate Cancer. *Front Oncol* 2022; **12**: 831429 [PMID: 35155262 DOI: 10.3389/fonc.2022.831429]
- 38 **Siva S**, Udovicich C, Tran B, Zargar H, Murphy DG, Hofman MS. Expanding the role of small-molecule PSMA ligands beyond PET staging of prostate cancer. *Nat Rev Urol* 2020; **17**: 107-118 [PMID: 31937920 DOI: 10.1038/s41585-019-0272-5]
- 39 **Zamboglou C**, Carles M, Fechter T, Kiefer S, Reichel K, Fassbender TF, Bronsert P, Koeber G, Schilling O, Ruf J, Werner M, Jilg CA, Baltas D, Mix M, Grosu AL. Radiomic features from PSMA PET for non-invasive intraprostatic tumor discrimination and characterization in patients with intermediate- and high-risk prostate cancer - a comparison study with histology reference. *Theranostics* 2019; **9**: 2595-2605 [PMID: 31131055 DOI: 10.7150/thno.32376]
- 40 **Nishino M**, Hayakawa K, Minami M, Yamamoto A, Ueda H, Takasu K. Primary retroperitoneal neoplasms: CT and MR imaging findings with anatomic and pathologic diagnostic clues. *Radiographics* 2003; **23**: 45-57 [PMID: 12533639 DOI: 10.1148/rg.231025037]
- 41 **Nickols N**, Anand A, Johnsson K, Brynolfsson J, Borreli P, Parikh N, Juarez J, Jafari L, Eiber M, Rettig M. aPROMISE: A Novel Automated PROMISE Platform to Standardize Evaluation of Tumor Burden in (18)F-DCFPyL Images of Veterans with Prostate Cancer. *J Nucl Med* 2022; **63**: 233-239 [PMID: 34049980 DOI: 10.2967/jnumed.120.261863]
- 42 **Johnsson K**, Brynolfsson J, Sahlstedt H, Nickols NG, Rettig M, Probst S, Morris MJ, Bjartell A, Eiber M, Anand A. Analytical performance of aPROMISE: automated anatomic contextualization, detection, and quantification of [(18)F]DCFPyL (PSMA) imaging for standardized reporting. *Eur J Nucl Med Mol Imaging* 2022; **49**: 1041-1051 [PMID: 34463809 DOI: 10.1007/s00259-021-05497-8]

Retrospective Cohort Study

Chronic thromboembolic pulmonary hypertension is associated with a loss of total lung volume on computed tomography

Nanae Tsuchiya, Yan-Yan Xu, Junji Ito, Tsuneo Yamashiro, Hidekazu Ikemiyagi, David Mummy, Mark L Schiebler, Koji Yonemoto, Sadayuki Murayama, Akihiro Nishie

Specialty type: Radiology, nuclear medicine and medical imaging

Provenance and peer review: Invited article; Externally peer reviewed.

Peer-review model: Single blind

Peer-review report's scientific quality classification

Grade A (Excellent): 0
Grade B (Very good): B, B
Grade C (Good): 0
Grade D (Fair): 0
Grade E (Poor): 0

P-Reviewer: Chen Q, China; Sharma D, India

Received: November 26, 2022

Peer-review started: November 26, 2022

First decision: March 15, 2023

Revised: April 4, 2023

Accepted: April 24, 2023

Article in press: April 24, 2023

Published online: May 28, 2023



Nanae Tsuchiya, Junji Ito, Sadayuki Murayama, Akihiro Nishie, Department of Radiology, Graduate School of Medical Science, University of the Ryukyus, Nishihara 903-0125, Okinawa, Japan

Yan-Yan Xu, Department of Radiology, China-Japan Friendship Hospital, Beijing 100029, China

Tsuneo Yamashiro, Department of Radiology, Yokohama City University, Yokohama 2360027, Japan

Hidekazu Ikemiyagi, Department of Cardiovascular Medicine, Nephrology and Neurology, Graduate School of Medicine, University of the Ryukyus, Nishihara 9030125, Okinawa, Japan

David Mummy, Center for In Vivo Microscopy and Department of Radiology, Duke University, Durham, NC 27710, United States

Mark L Schiebler, Department of Radiology, University of Wisconsin-Madison, Madison, WI 53792, United States

Koji Yonemoto, Department of Biostatistics, School of Health Sciences, Faculty of Medicine, University of the Ryukyus, Nishihara 903-0215, Okinawa, Japan

Corresponding author: Nanae Tsuchiya, MD, PhD, Lecturer, Department of Radiology, Graduate School of Medical Science, Tsuchiya, N (reprint author), Graduate School of Medical Science, University of the Ryukyus, 207 Uehara, Nishihara-Cho, Nakagami-Gun, Okinawa 903-0215, Japan. nanae7a50@hotmail.com

Abstract**BACKGROUND**

Although lung volumes are usually normal in individuals with chronic thromboembolic pulmonary hypertension (CTEPH), approximately 20%-29% of patients exhibit a restrictive pattern on pulmonary function testing.

AIM

To quantify longitudinal changes in lung volume and cardiac cross-sectional area (CSA) in patients with CTEPH.

METHODS

In a retrospective cohort study of patients seen in our hospital between January

2012 and December 2019, we evaluated 15 patients with CTEPH who had chest computed tomography (CT) performed at baseline and after at least 6 mo of therapy. We matched the CTEPH cohort with 45 control patients by age, sex, and observation period. CT-based lung volumes and maximum cardiac CSAs were measured and compared using the Wilcoxon signed-rank test and the Mann-Whitney *u* test.

RESULTS

Total, right lung, and right lower lobe volumes were significantly reduced in the CTEPH cohort at follow-up *vs* baseline (total, $P = 0.004$; right lung, $P = 0.003$; right lower lobe; $P = 0.01$). In the CTEPH group, the reduction in lung volume and cardiac CSA was significantly greater than the corresponding changes in the control group (total, $P = 0.01$; right lung, $P = 0.007$; right lower lobe, $P = 0.01$; CSA, $P = 0.0002$). There was a negative correlation between lung volume change and cardiac CSA change in the control group but not in the CTEPH cohort.

CONCLUSION

After at least 6 mo of treatment, CT showed an unexpected loss of total lung volume in patients with CTEPH that may reflect continued parenchymal remodeling.

Key Words: Pulmonary hypertension; Lung; Computed tomography; Retrospective study; Lung volume measurements; Follow-up studies

©The Author(s) 2023. Published by Baishideng Publishing Group Inc. All rights reserved.

Core Tip: The total lung volume, right lower lobe volume, and cardiac cross-sectional area were reduced after at least 6 mo of follow-up after treatment in patients with chronic thromboembolic pulmonary hypertension (CTEPH). This finding suggests that structural lung changes have occurred in CTEPH, possibly from continued infarction with secondary volume loss from fibrosis or bronchoconstriction. The loss of lung volume may prove to be an important clinical consideration in CTEPH treatment because pulmonary function may continue to deteriorate despite improved right heart function in patients with CTEPH.

Citation: Tsuchiya N, Xu YY, Ito J, Yamashiro T, Ikemiyagi H, Mummy D, Schiebler ML, Yonemoto K, Murayama S, Nishie A. Chronic thromboembolic pulmonary hypertension is associated with a loss of total lung volume on computed tomography. *World J Radiol* 2023; 15(5): 146-156

URL: <https://www.wjgnet.com/1949-8470/full/v15/i5/146.htm>

DOI: <https://dx.doi.org/10.4329/wjr.v15.i5.146>

INTRODUCTION

Chronic thromboembolic pulmonary hypertension (CTEPH) is characterized by the presence of residual organized thrombi and vascular remodeling, leading to progressive pulmonary hypertension and right ventricular failure[1]. Surgical pulmonary endarterectomy (PEA) is a treatment for surgically accessible CTEPH. However, it has been reported that 17%-25% of patients undergoing PEA have residual or recurrent pulmonary hypertension[2]. In addition, approximately 30% of patients are not eligible for PEA because of the distal location of their pulmonary thromboemboli[3]; balloon pulmonary angioplasty (BPA) or medical therapy are the preferred treatment strategies for such patients[1,4,5].

Spirometry results and lung volumes are usually normal in patients with CTEPH, but approximately 20%-29% of patients exhibit a restrictive pattern on pulmonary function testing[6-8]. This reduction in lung volume is thought to be caused by parenchymal scarring from pulmonary infarction and not by displacement from proximal vessel hypertrophy and dilatation[7].

The nature of the progression of this observed reduction in lung volume in patients with CTEPH has not previously been described[3,9]. In our practice, we sometimes encounter patients who are receiving BPA or medical treatment for CTEPH but are gradually losing lung volume on chest computed tomography (CT); these patients require long-term follow-up. Based on this experience, we hypothesized that lung volume decreases over time in patients with CTEPH who have not undergone PEA. Furthermore, since heart size can be increased in patients with CTEPH and right heart failure, we suspected that this cardiomegaly might be another potential and as yet unreported contributor to the lung volume reduction seen in CTEPH.

The purpose of this study was to investigate longitudinal changes in CT lung volume and to evaluate the relationship between lung volume and heart size in patients with CTEPH.

MATERIALS AND METHODS

Our institutional review board approved this retrospective cohort study and waived the requirement for patient informed consent.

Patients

We conducted a retrospective review of patients seen at our institution between January 2012 and December 2019. Patients were initially identified using a picture archiving and communications system database, and patient selection was further refined by reviewing the electronic medical records. The inclusion criteria were a clinical diagnosis of CTEPH, age between 20 years and 90 years, chest CT performed at initial diagnosis and at the time of follow-up, and a minimum 6-mo interval between CT imaging sessions (Figure 1). We excluded patients who underwent PEA, patients for whom there was a lack of thin-slice CT images (< 2 mm) or poor image quality (*e.g.*, motion artifact from a missed breath hold), and patients with other conditions that might affect lung volume (*e.g.*, pleural effusion, underlying chronic pulmonary disease such as emphysema, interstitial lung disease, or old tuberculosis, and a history of thoracic surgery). The inclusion criterion for individuals in the control group, which was matched by age, sex, and observation period, was the presence of two chest CTs performed to observe cancer status (renal or prostate cancer for men; uterine cancer for women). Individuals were excluded from the control group if there was a lack of thin-slice CT images, poor image quality, or any abnormal findings on chest CT.

The diagnosis of CTEPH was determined by cardiologists based on a detailed medical history, physical examination, chest radiography, chest CT, echocardiography, lung ventilation–perfusion scintigraphy, right heart catheterization (RHC), and angiographic demonstration of multiple stenoses and obstruction of bilateral pulmonary arteries[10]. Radiologist reports were reviewed to determine which pulmonary arteries were affected by chronic thrombosis. Clinical data, including age, height, weight, and treatment details (*e.g.*, anticoagulant therapy, BPA), were extracted from the medical records. We also noted the results of RHC (mean pulmonary arterial pressure, cardiac output, cardiac index) and echocardiography (tricuspid regurgitation pressure gradient, left ventricular end-diastolic diameter, left ventricular end-systolic diameter) at the examination closest in time to the chest CT.

Computed tomography

Chest CT, with or without contrast, was performed as part of routine clinical practice. Two scanners were used: The Light Speed VCT 64-row CT (GE HealthCare, Milwaukee, WI, United States) and the Aquilion ONE 320-row CT (Canon Medical Systems, Odawara, Japan). Imaging was performed during a supine breath-hold at full inspiration. Instructions for full inspiration were given using an automatic voice system to keep the degree of inspiration constant. The imaging parameters were: Voltage, 120 kVp; current, automatic exposure control; collimation, 0.5 (Canon) or 0.625 mm (GE); rotation time, 0.5 sec; matrix, 512 × 512; and slice thicknesses, 1 mm (Canon) or 1.25 mm (GE).

Image analysis

Lung volumes were automatically segmented and calculated using a commercially available workstation (SYNAPSE VINCENT, version 4.1; Fujifilm Healthcare Corporation, Tokyo, Japan). We used images with a soft tissue reconstruction algorithm [Standard (GE) or FC14 (Canon)] for analysis. Lung volumes were assessed based on lobe anatomy: Right upper and middle lobe; right lower lobe; left upper lobe; and left lower lobe. The right upper and middle lobes were assessed together because of the frequent presence of incomplete lobulation.

We calculated the amount of change in lung volume between the initial CT and follow-up CT. The slice with the maximal cardiac cross-sectional area (CSA) in cm² was measured semiautomatically using a commercially available workstation (SYNAPSE VINCENT, version 4.1). Based on a previously published method[11], the following process was used for each patient. A Hounsfield unit threshold was set to exclude the pericardial fat pad (0–300 Hounsfield unit). All images that contained the heart were then identified, and the maximum cardiac CSA was determined. Finally, the boundary of the heart was traced, and the maximum cardiac CSA recorded. In addition, we calculated the size change (difference in area) in cardiac CSA between the initial and follow-up CT images. Lung volume and cardiac CSA were analyzed separately by different radiologists (NT and YX) who were blinded to the patients' clinical information (Figure 1).

Statistical analysis

The sample size for this study was determined by the following method[12]: Average lung volume, 2000 mL; standard deviation, 400 mL; effect size, 400 mL (20% of average); patient to control ratio, 1:3; α , 0.05; and power, 0.8.

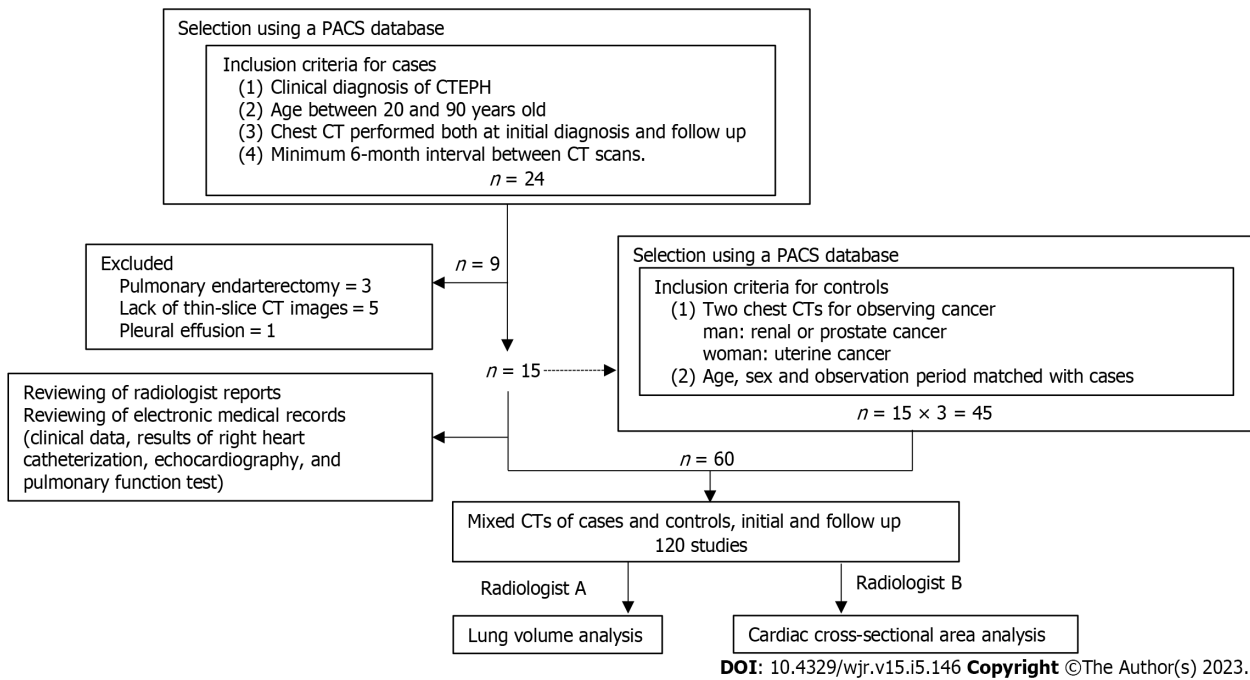


Figure 1 Study flow chart. CT: Computed tomography; CTEPH: Chronic thromboembolic pulmonary hypertension; PACS: Picture archiving and communications system.

Statistical analyses were performed using JMP 11 (SAS Institute Japan, Tokyo, Japan). Continuous variables were calculated as the mean and 95% confidence interval. The Wilcoxon signed-rank test was used to compare parameters between the initial and follow-up CT for both groups. The Mann-Whitney *U* test was used to compare parameters between patients with CTEPH and those in the control group. The Spearman correlation coefficient was used to determine the correlation between lung volume and cardiac CSA. A *P* value of less than 0.05 was considered statistically significant.

RESULTS

We identified 27 individuals with CTEPH who were seen during the study period. Of these, 24 had two chest CTs with an interval greater than 6 mo. We excluded 3 patients who underwent PEA, 5 patients who lacked thin-slice CT images, and 1 patient with a pleural effusion. The size of the CTEPH population was thus fixed at 15 (4 males and 11 females) due to the retrospective nature of the study. The mean patient age was 48 years (range: 40–83 years). The size of the control group was set at 45 individuals (3 times the size of the CTEPH group). All individuals with CTEPH received anticoagulant therapy, and 14 patients underwent BPA. Patient characteristics are summarized in [Table 1](#). The results of echocardiography and RHC performed before and after therapy are shown in [Table 2](#).

Comparison between initial and follow-up measurements of lung volume and cardiac CSA

The initial and follow-up measurements for lung volume are shown in [Table 2](#). The total lung volume ($P = 0.004$), right lung volume ($P = 0.003$), and the right lower lobe volume ($P = 0.01$) at total lung capacity (TLC) were significantly reduced in patients with CTEPH at follow-up ([Figures 2 and 3](#)), but there were no significant longitudinal changes in lung volumes in the control group. The cardiac CSA was significantly reduced in the CTEPH cohort at follow-up ($P = 0.001$), but this change was not observed in the control group.

Comparison between measures of lung volume and cardiac CSA in patients with CTEPH vs controls

The lung volumes and cardiac CSA measurements for the CTEPH cohort and the control group are shown in [Table 3](#). There was no significant difference in lung volumes between groups, but the cardiac CSA was larger in the CTEPH group than in the control group at both initial and follow-up assessments ($P < 0.0001$). In the CTEPH cohort, the reduction in total lung volume ($P = 0.01$) and in right lung volume ($P = 0.007$) and right lower lobe volume ($P = 0.01$) was significantly larger than that seen in the control group ([Figure 4](#)). The reduction in cardiac CSA in the CTEPH cohort was significantly greater than in the control group ($P = 0.0002$).

Table 1 Population characteristics

Characteristic	CTEPH, <i>n</i> = 15		Control, <i>n</i> = 45	<i>P</i> value
Age in yr, mean (95%CI)	48 (40, 83)		48 (40, 83)	-
Height in cm, mean (95%CI)	159 (151, 162)		159 (154, 163)	0.5
Weight in kg, mean (95%CI)	58 (49, 75)		61 (54, 72)	0.9
Interval between initial and follow-up CT in d, mean (95%CI)	547 (273, 846)		531 (294, 815)	0.9
Results of RHC and echocardiography	Initial, <i>n</i> = 15	Follow-up, <i>n</i> = 15		<i>P</i> value
Pulmonary arterial pressure in mmHg, mean (95%CI)	47 (38, 59)	34 (23, 44)	-	0.001 ^b
Cardiac output in L/min, mean (95%CI)	3.4 (2.8, 4.3)	4.6 (3.6, 6.1)	-	0.01 ^a
Cardiac index in L/min/m ² , mean (95%CI)	2.2 (1.6, 2.7)	2.7 (2.4, 3.6)	-	0.01 ^a
Tricuspid regurgitation pressure gradient in mmHg, mean (95%CI)	66 (51, 77)	42 (23, 61)	-	0.01 ^a
Left ventricular end-diastolic diameter in mm, mean (95%CI)	38 (37, 42)	44 (41, 47)	-	0.02 ^a
Left ventricular end-systolic diameter in mm, mean (95%CI)	25 (22, 28)	27 (24, 31)	-	0.5
Results of spirometry	Initial, <i>n</i> = 10	Follow-up, <i>n</i> = 10		
Vital capacity % predicted	83 (70, 102)	87 (76, 99)	-	0.2
Forced vital capacity % predicted	76 (71, 97)	83 (74, 97)	-	0.3
Forced expiratory volume-one second % predicted	74 (63, 95)	83 (69, 96)	-	0.5

^a*P* < 0.05.^b*P* < 0.01. CI: Confidence interval; CT: Computed tomography; CTEPH: Chronic thromboembolic pulmonary hypertension; RHC: Right heart catheterization.**Table 2 Comparison between measurements on initial and follow-up computed tomography**

CT measurement	CTEPH, <i>n</i> = 15			Control, <i>n</i> = 45		
	Initial	Follow-up	<i>P</i> value	Initial	Follow-up	<i>P</i> value
Total lung volume in mL, mean (95%CI)	3238 (3016, 4494)	3360 (2687, 4043)	0.004 ^b	3669 (3063, 4167)	3657 (2993, 4385)	0.9
Right lung volume in mL, mean (95%CI)	1879 (1700, 2619)	1817 (1522, 2299)	0.003 ^b	1939 (1635, 2268)	1990 (1614, 2347)	0.9
Right upper + middle lobe volume in mL, mean (95%CI)	977 (913, 1103)	973 (900, 1148)	0.2	1028 (868, 1169)	1010 (865, 1212)	1.0
Right lower lobe lung volume in mL, mean (95%CI)	978 (737, 1123)	815 (611, 1111)	0.01 ^a	931 (707, 1112)	911 (733, 1148)	0.8
Left lung volume in mL, mean (95%CI)	1396 (1316, 1875)	1455 (1216, 1744)	0.1	1692 (1376, 1940)	1659 (1403, 2023)	0.7
Left upper lobe lung volume in mL, mean (95%CI)	836 (752, 925)	802 (689, 1000)	0.4	867 (747, 1042)	869 (741, 1089)	0.9
Left lower lobe lung volume in mL, mean (95%CI)	636 (555, 902)	652 (476, 806)	0.05	826 (628, 939)	749 (622, 999)	0.6
Heart cross-sectional area in cm ² , mean (95%CI)	97 (86, 112)	83 (69, 100)	0.001 ^b	75 (65, 85)	74 (64, 85)	0.7

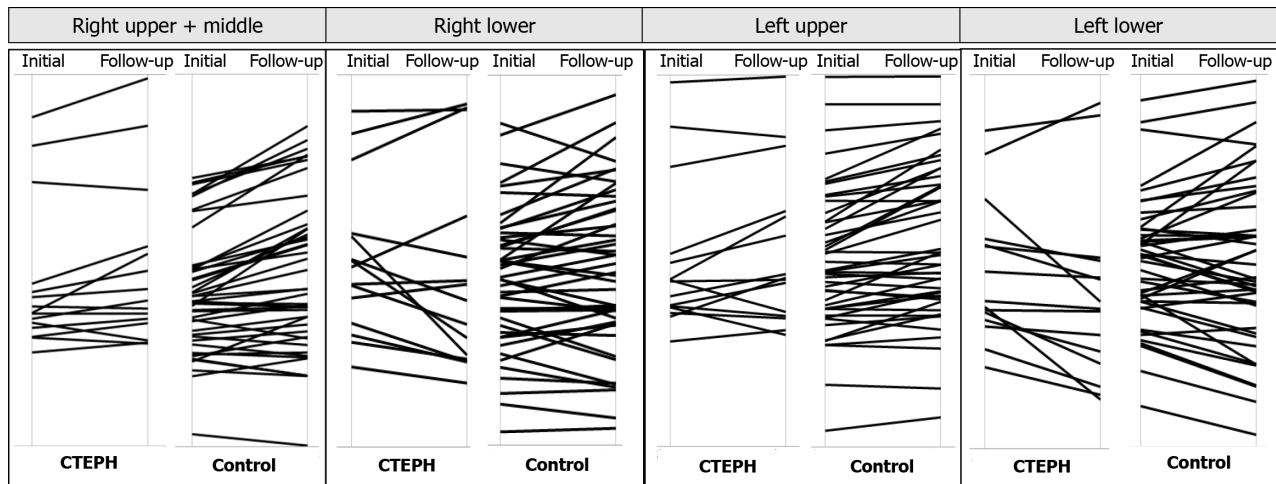
^a*P* < 0.05.^b*P* < 0.01. CI: Confidence interval; CT: Computed tomography; CTEPH: Chronic thromboembolic pulmonary hypertension.

Correlation between lung volume and cardiac CSA

There were no significant correlations between lung volume and cardiac CSA in the CTEPH cohort or the control group at either initial or follow-up CT. In the CTEPH group, there were no significant correlations between lung volume change and the change in cardiac CSA. In the control group, the change in cardiac CSA was negatively correlated with total lung volume change ($\rho = -0.44$; $P = 0.002$), right lung volume change ($\rho = -0.34$; $P = 0.01$), right upper and middle lobe volume change ($\rho = -0.27$; $P = 0.06$), right lower lobe volume change ($\rho = -0.34$; $P = 0.02$), left lung volume change ($\rho = -0.50$; $P = 0.0004$), left upper lobe volume change ($\rho = -0.40$; $P = 0.0005$), and left lower lobe volume change ($\rho = -0.52$; $P = 0.0002$) (Figure 5).

Table 3 Lung volume and heart-size change in patients with chronic thromboembolic pulmonary hypertension and in the control group

Parameter	CTEPH, n = 15	Control, n = 45	P value
Total lung volume change in mL, mean (95%CI)	176 (13, 468)	39 (-228, 252)	0.01 ^a
Right lung volume change in mL, mean (95%CI)	120 (47, 292)	4 (-121, 126)	0.007 ^b
Right upper + middle lobe lung volume change in mL, mean (95%CI)	35 (-26, 91)	-7 (-46, 46)	0.9
Right lower lobe lung volume change in mL, mean (95%CI)	85 (19, 167)	-9 (-66, 83)	0.01 ^a
Left lung volume change in mL, mean (95%CI)	23 (-37, 214)	33 (-109, 99)	0.1
Left upper lobe lung volume change in mL, mean (95%CI)	13 (-31, 81)	1 (-44, 53)	0.4
Left lower lobe lung volume change in mL, mean (95%CI)	40 (-23, 112)	9 (-59, 63)	0.1
Cardiac cross-sectional area change in cm ² , mean (95%CI)	19 (4, 25)	-0.3 (-2, 3)	0.0002 ^c

^aP < 0.05.^bP < 0.01.^cP < 0.001. CI: Confidence interval; CTEPH: Chronic thromboembolic pulmonary hypertension.

DOI: 10.4329/wjr.v15.i5.146 Copyright ©The Author(s) 2023.

Figure 2 Parallel plots between initial computed tomography and follow-up computed tomography. The right lower lung volume decreased significantly over time in the chronic thromboembolic pulmonary hypertension (CTEPH) group. There were no significant changes in lung volume in the control group.

DISCUSSION

This pilot study showed that the lung volume in patients with CTEPH who are treated medically decreases over 6 mo of follow-up, despite a reduction in heart size during that same period. These results suggest that a reduction in lung volume may continue in patients with CTEPH who have not undergone PEA, and that this reduction may occur independently of right heart enlargement quantified using cardiac CSA.

Although decreased TLC has been previously observed in patients with CTEPH[7], this report analyzed regional contributions to reduction in lung volume using CT measurements, showing that the right lung and right lower lung have significantly reduced volumes. The reason for this may be related to continued lung remodeling and loss of parenchyma from continuing pulmonary infarction. Reports of pulmonary embolism show a striking lower lobe predominance, with an embolus rate in the right lower lobe twice that of the left lower lobe[13]. Thus, it is plausible that the right lower lung is a major contributor to lung volume reduction because of its status as a predominant region of pulmonary infarction.

A retrospective study by Morris *et al*[7] found that 22% of the 51 patients with CTEPH who were candidates for PEA had restrictive lung disease on pulmonary function testing, defined as a TLC less than 80% of predicted. They also demonstrated that the reduction in lung volume was correlated to the degree of parenchymal scarring occurring after pulmonary infarction. Pulmonary infarction is more common with peripheral pulmonary emboli than with central pulmonary emboli due to the relatively lower contribution of bronchial arterial supply to the peripheral lung[13,14].

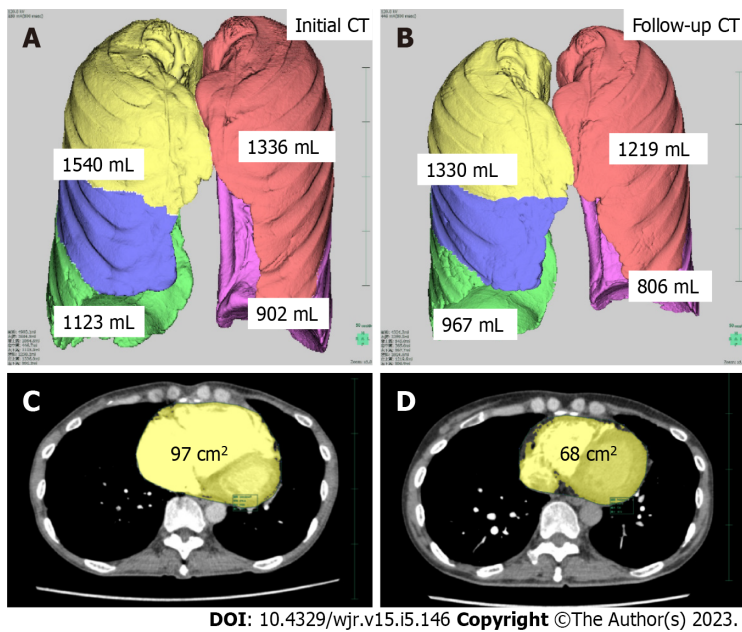


Figure 3 A 55-year-old female with chronic thromboembolic pulmonary hypertension was observed for 15 mo. A: The lung lobar volumes before treatment; B: The lung lobar volumes after treatment showed a loss of volume from both lung bases; C: The cardiac cross-sectional area was improved after balloon pulmonary angioplasty; D: The right ventricle returned to a normal size. CT: Computed tomography.

The decline in heart size seen with CTEPH is most likely related to the improvement in right ventricular function and decreased right ventricular end-diastolic and end-systolic volumes with medical therapy or BPA. Echocardiography and RHC show these improvements at follow-up. Cardiac CSA, measured in the transverse plane, is affected by the phase of ventilation. Inhalation stretches the heart in the vertical plane and reduces cardiac CSA, whereas expiration lifts the diaphragm and pushes the heart upward, increasing cardiac CSA[11]. The control group in this study had a significant negative correlation between heart size change, as measured by CSA, and lung volume change. However, the correlation between these changes disappeared in the CTEPH cohort. We initially speculated that cardiomegaly was a factor in lung volume decline in the CTEPH group. In addition to the physiologic increase in cardiac CSA caused by poor inspiration, the increase in the right ventricle and right atrium volume caused by exacerbation of right heart failure would compress the lung parenchyma, leading to a decrease in lung volume. However, we found the opposite to be true: lung volumes decreased in the CTEPH group despite a reduction in heart size. In other words, a reduction in heart size that is associated with improved heart function can occur simultaneously with a loss of lung volume in CTEPH. An additional explanation of this negative correlation between heart size and lung volume is that in normal individuals more vigorous inspiration when measuring TLC reduces venous filling of the right atrium. In patients with CTEPH, there should be less of an effect because these individuals already have volume overload in the right heart.

There have been remarkable recent advances in treatment for inoperable CTEPH, and survival has significantly improved in the population treated with medication or BPA[2]. However, whether quality of life improves after medical therapy has been controversial, and there have been no reports of changes in quality of life following BPA[15-19]. While TLC reportedly increases following BPA for CTEPH[20], this is only a short-term outcome. Further study is needed to clarify whether this temporary increase in lung volume and subsequent regression may influence quality of life in patients with CTEPH.

There are several limitations to this study. First, this is a retrospective single-center study with a small number of patients, and spirometry data are lacking. Second, height is an important factor influencing lung volume, but this was not matched between patients in the CTEPH and control groups; however, mean height was not significantly different between the groups. Therefore, this effect is likely to be negligible. Third, there were multiple hardware vendors for the CT scanners used in this project. Finally, the absolute inspiration volume for CT was not measured with spirometry.

CONCLUSION

The total lung volume, right lower lobe volume, and the cardiac CSA were reduced after at least 6 mo of follow-up after treatment in patients with CTEPH. This finding suggests that structural changes in the lung have occurred, possibly from continued infarction with secondary volume loss from fibrosis or bronchoconstriction. The results of this study suggest that pulmonary function may continue to

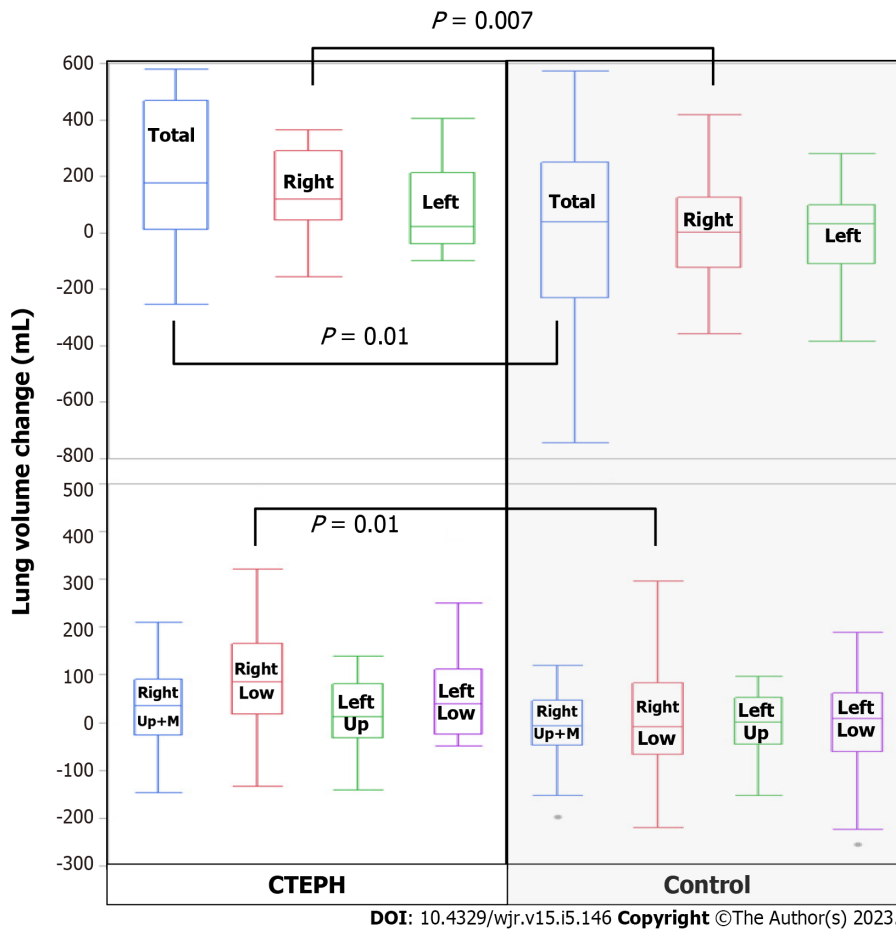


Figure 4 Box and whisker plots of individuals with chronic thromboembolic pulmonary hypertension and individuals in the control group. There were significant changes over time in the total lung, right lung, and right lower lobe but not the right upper and middle lobes. There was no significant change in volume in the left lung, left upper lobe, or left lower lobe. CTEPH: Chronic thromboembolic pulmonary hypertension; Up: Upper lobe; M: Middle lobe; Low: Lower lobe.

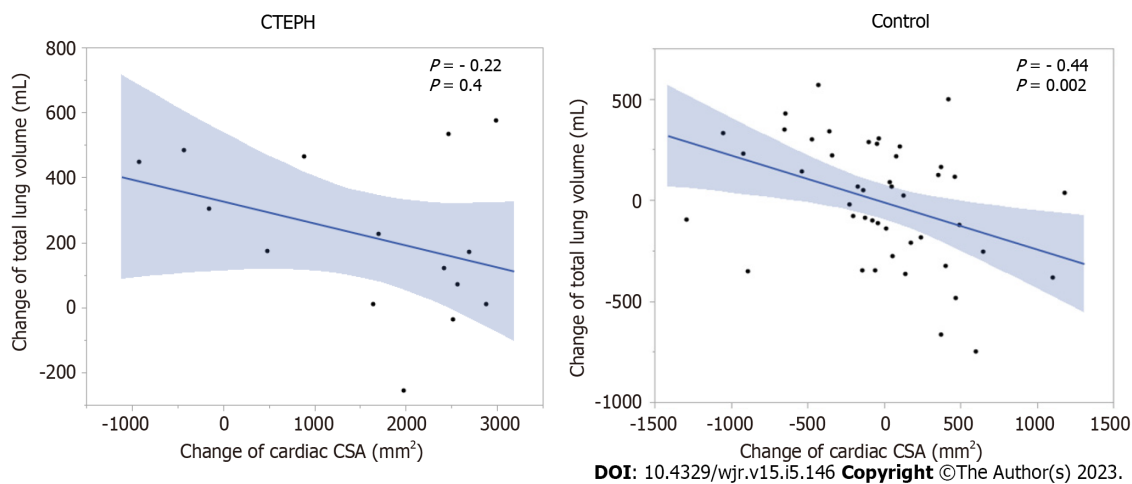


Figure 5 Relationship between lung volume change and cardiac cross-sectional area in patients with chronic thromboembolic pulmonary hypertension group and in the control group. There was a negative correlation between total lung volume and cardiac cross-sectional area (CSA) in the control group but not in the chronic thromboembolic pulmonary hypertension (CTEPH) group.

deteriorate in patients with CTEPH despite improvements in right heart function and decreased right ventricular volumes from lowered pulmonary arterial pressure after treatment. This loss of lung volume may prove to be an important clinical consideration in CTEPH treatment.

ARTICLE HIGHLIGHTS

Research background

In chronic thromboembolic pulmonary hypertension (CTEPH), about 20% of patients have lung restriction due to parenchymal scarring. We sometimes follow CTEPH patients who gradually lose lung volume. There is no report describing the temporal change in lung volume of CTEPH patients.

Research motivation

The loss of lung volume may be an important clinical consideration in CTEPH treatment.

Research objectives

The purpose of this study was to assess the temporal lung volume changes in CTEPH.

Research methods

Included in the study were patients with CTEPH who underwent two thoracic computed tomography (CT) examinations with a between-test interval that was greater than 6 mo. We also assessed controls matched by age, sex, and observation period. The lung volume was measured on the left and right sides by thin-slice CT scanning. Lung volume was automatically measured by lung analysis software. We analyzed the lung volume changes between the initial CT and follow-up CT in patients and controls by the Wilcoxon signed-rank test.

Research results

The total and right lung volumes were significantly reduced from the initial CT to the follow-up CT in the patients with CTEPH. In CTEPH patients, there was no significant change in the left lung volume. In controls, there were no significant changes in lung volume.

Research conclusions

In patients with CTEPH, the lung volume was reduced temporally. The right lung was more affected than the left lung by the lung volume reduction.

Research perspectives

Further study is needed to clarify whether this temporary increase in lung volume and subsequent regression may influence quality of life in patients with CTEPH.

ACKNOWLEDGEMENTS

The authors are grateful to Ms. Chihiro Siroma for contribution to collection of the data.

FOOTNOTES

Author contributions: All authors contributed to the study conception and design; Tsuchiya N, Xu YY, and Ito J performed the data collection and image interpretation; Tsuchiya N and Yonemoto K performed the statistical analysis; Tsuchiya N wrote the first draft of the manuscript; and all authors commented on previous versions of the manuscript and read and approved the final manuscript.

Supported by The Japan Society for the Promotion of Science, No. 24591782.

Institutional review board statement: This study was approved by the Ethics Committee for Clinical Research of University of the Ryukyus with waiver of informed consent (Approval No., 1039).

Informed consent statement: Our institutional review board approved this retrospective cohort study and waived the requirement for patient informed consent.

Conflict-of-interest statement: All authors report having no relevant conflicts of interest for this article.

Data sharing statement: The original anonymous dataset is available upon request from the corresponding author at nanae7a50@hotmail.com.

Open-Access: This article is an open-access article that was selected by an in-house editor and fully peer-reviewed by external reviewers. It is distributed in accordance with the Creative Commons Attribution NonCommercial (CC BY-NC 4.0) license, which permits others to distribute, remix, adapt, build upon this work non-commercially, and license their derivative works on different terms, provided the original work is properly cited and the use is non-

commercial. See: <https://creativecommons.org/licenses/by-nc/4.0/>

Country/Territory of origin: Japan

ORCID number: Nanae Tsuchiya 0000-0003-2556-8287; Mark L Schiebler 0000-0002-9120-5428; Akihiro Nishie 0000-0001-7103-7757.

S-Editor: Liu XF

L-Editor: Filipodia

P-Editor: Zhao S

REFERENCES

- 1 **Robbins IM**, Pugh ME, Hemnes AR. Update on chronic thromboembolic pulmonary hypertension. *Trends Cardiovasc Med* 2017; **27**: 29-37 [PMID: 27345156 DOI: 10.1016/j.tcm.2016.05.010]
- 2 **Miwa H**, Tanabe N, Jujo T, Kato F, Anazawa R, Yamamoto K, Naito A, Kasai H, Nishimura R, Suda R, Sugiura T, Sakao S, Ishida K, Masuda M, Tatsumi K. Long-Term Outcome of Chronic Thromboembolic Pulmonary Hypertension at a Single Japanese Pulmonary Endarterectomy Center. *Circ J* 2018; **82**: 1428-1436 [PMID: 29540628 DOI: 10.1253/circj.CJ-17-1242]
- 3 **Low AT**, Medford AR, Millar AB, Tulloh RM. Lung function in pulmonary hypertension. *Respir Med* 2015; **109**: 1244-1249 [PMID: 26033642 DOI: 10.1016/j.rmed.2015.05.022]
- 4 **Moriarty JM**, Khan SN, Kao SD, Saggarr R. Balloon Pulmonary Angioplasty for Chronic Thromboembolic Pulmonary Hypertension. *Cardiovasc Intervent Radiol* 2018; **41**: 1826-1839 [PMID: 30039506 DOI: 10.1007/s00270-018-2012-2]
- 5 **Aoki T**, Sugimura K, Tatebe S, Miura M, Yamamoto S, Yaoita N, Suzuki H, Sato H, Koza K, Konno R, Miyata S, Nochioka K, Satoh K, Shimokawa H. Comprehensive evaluation of the effectiveness and safety of balloon pulmonary angioplasty for inoperable chronic thrombo-embolic pulmonary hypertension: long-term effects and procedure-related complications. *Eur Heart J* 2017; **38**: 3152-3159 [PMID: 29029023 DOI: 10.1093/eurheartj/ehx530]
- 6 **Horn M**, Ries A, Neveu C, Moser K. Restrictive ventilatory pattern in precapillary pulmonary hypertension. *Am Rev Respir Dis* 1983; **128**: 163-165 [PMID: 6870057 DOI: 10.1164/arrd.1983.128.1.163]
- 7 **Morris TA**, Auger WR, Ysrael MZ, Olson LK, Channick RN, Fedullo PF, Moser KM. Parenchymal scarring is associated with restrictive spirometric defects in patients with chronic thromboembolic pulmonary hypertension. *Chest* 1996; **110**: 399-403 [PMID: 8697841 DOI: 10.1378/chest.110.2.399]
- 8 **Fukushi K**, Kataoka M, Shimura N, Inami T, Fukuda K, Yoshino H, Satoh T. Impaired Respiratory Function in Chronic Thromboembolic Pulmonary Hypertension: A Comparative Study with Healthy Control Subjects. *Ann Am Thorac Soc* 2016; **13**: 1183-1184 [PMID: 27388407 DOI: 10.1513/AnnalsATS.201601-048LE]
- 9 **Kahn SR**, Houweling AH, Granton J, Rudski L, Dennie C, Hirsch A. Long-term outcomes after pulmonary embolism: current knowledge and future research. *Blood Coagul Fibrinolysis* 2014; **25**: 407-415 [PMID: 24469387 DOI: 10.1097/MBC.0000000000000070]
- 10 **Kim NH**, Delcroix M, Jenkins DP, Channick R, Dartevelle P, Jansa P, Lang I, Madani MM, Ogino H, Pengo V, Mayer E. Chronic thromboembolic pulmonary hypertension. *J Am Coll Cardiol* 2013; **62**: D92-D99 [PMID: 24355646 DOI: 10.1016/j.jacc.2013.10.024]
- 11 **Tomita H**, Yamashiro T, Matsuoka S, Matsushita S, Kurihara Y, Nakajima Y. Changes in Cross-Sectional Area and Transverse Diameter of the Heart on Inspiratory and Expiratory Chest CT: Correlation with Changes in Lung Size and Influence on Cardiothoracic Ratio Measurement. *PLoS One* 2015; **10**: e0131902 [PMID: 26151361 DOI: 10.1371/journal.pone.0131902]
- 12 **Kohn MA**, Senyak J. Sample Size Calculators. 2021 December 20 [cited 24 January 2020]. San Francisco: UCSF CTSI [DOI: 10.3840/002042]
- 13 **He H**, Stein MW, Zalta B, Haramati LB. Pulmonary infarction: spectrum of findings on multidetector helical CT. *J Thorac Imaging* 2006; **21**: 1-7 [PMID: 16538148 DOI: 10.1097/01.rti.00000187433.06762.fb]
- 14 **Tsao MS**, Schraufnagel D, Wang NS. Pathogenesis of pulmonary infarction. *Am J Med* 1982; **72**: 599-606 [PMID: 6462058 DOI: 10.1016/0002-9343(82)90458-2]
- 15 **Mathai SC**, Ghofrani HA, Mayer E, Pepke-Zaba J, Nikkho S, Simonneau G. Quality of life in patients with chronic thromboembolic pulmonary hypertension. *Eur Respir J* 2016; **48**: 526-537 [PMID: 27076580 DOI: 10.1183/13993003.01626-2015]
- 16 **Scholzel BE**, Post MC, Thijs Plokker HW, Snijder RJ. Clinical worsening during long-term follow-up in inoperable chronic thromboembolic pulmonary hypertension. *Lung* 2012; **190**: 161-167 [PMID: 22160210 DOI: 10.1007/s00408-011-9350-z]
- 17 **Suntharalingam J**, Treacy CM, Doughty NJ, Goldsmith K, Soon E, Toshner MR, Sheares KK, Hughes R, Morrell NW, Pepke-Zaba J. Long-term use of sildenafil in inoperable chronic thromboembolic pulmonary hypertension. *Chest* 2008; **134**: 229-236 [PMID: 18263674 DOI: 10.1378/chest.07-2681]
- 18 **Jais X**, D'Armini AM, Jansa P, Torbicki A, Delcroix M, Ghofrani HA, Hoepfer MM, Lang IM, Mayer E, Pepke-Zaba J, Perchenet L, Morganti A, Simonneau G, Rubin LJ; Bosentan Effects in iNopErable Forms of chronIc Thromboembolic pulmonary hypertension Study Group. Bosentan for treatment of inoperable chronic thromboembolic pulmonary hypertension: BENEFIT (Bosentan Effects in iNopErable Forms of chronIc Thromboembolic pulmonary hypertension), a randomized, placebo-controlled trial. *J Am Coll Cardiol* 2008; **52**: 2127-2134 [PMID: 19095129 DOI: 10.1016/j.jacc.2008.08.059]

- 19 **Halank M**, Hoeper MM, Ghofrani HA, Meyer FJ, Stähler G, Behr J, Ewert R, Fletcher M, Colorado P, Nikkho S, Grimminger F. Riociguat for pulmonary arterial hypertension and chronic thromboembolic pulmonary hypertension: Results from a phase II long-term extension study. *Respir Med* 2017; **128**: 50-56 [PMID: 28610669 DOI: 10.1016/j.rmed.2017.05.008]
- 20 **Takei M**, Kataoka M, Kawakami T, Kuwahira I, Fukuda K. Respiratory function and oxygenation after balloon pulmonary angioplasty. *Int J Cardiol* 2016; **212**: 190-191 [PMID: 27038731 DOI: 10.1016/j.ijcard.2016.03.061]



Published by **Baishideng Publishing Group Inc**
7041 Koll Center Parkway, Suite 160, Pleasanton, CA 94566, USA
Telephone: +1-925-3991568
E-mail: bpgoffice@wjgnet.com
Help Desk: <https://www.f6publishing.com/helpdesk>
<https://www.wjgnet.com>

